ChemCatChem

Research Article
doi.org/10.1002/cctc.202400179

Chemistry
Europe
European Chemical
Societies Publishing

www.chemcatchem.org

Modified Halloysite as Catalyst for the Conversion of Hydroxymethylfurfural to Furandicarboxylic Acid: A DFT Investigation

Marco Bertini,[a] Francesco Ferrante,*[a] Ludovico Guercio,[a] Lorenzo Lisuzzo,[a] and Dario Duca[a]

The reaction steps involved in the 5-hydroxymethylfurfural to 2,5-furandicarboxylic acid conversion by means of H_2O_2 were investigated employing a dedicated computational protocol based on density functional theory. The catalytic environment of choice was a molecular model representing a portion of the halloysite nanotube outer surface, functionalized by an organo-silane, the 3-aminopropyltriethoxysilane, whose amino group bonds one gold atom. At this stage of the investigation, the process was fully detailed in terms of the interactions between the reaction intermediates and the catalyst, and the reaction standard free energies. In addition, the energy barriers of the elementary steps involving the hydrogen migration from the adsorbed organic species to the gold atom were analyzed. On the basis of the interaction geometries, a certain distinction among the preferred reaction path can be inferred as a function of the net negative charge characterizing the catalyst outer surface. Since the inner surface of halloysite can represent the acid environment needed to obtain 5-hydroxymethylfurfural through dehydration of fructose, the present study is framed in a wider research field where the possibility to consider functionalized halloysite as one-pot reactor for the valorization of biomass is explored.

Introduction

The increasing demand for a sustainable approach to produce environmentally friendly polymers that could replace the already existing petroleum-based plastics has led the attention of researchers on the synthesis of 2,5-furandicarboxylic acid (FDCA).[1] Due to the unique cyclic furan ring bearing diacid group, FDCA is indeed considered as the most promising precursor in the furan family for the production of green polymers, starting from the conversion of biomass into sugars.[2,3] In 2004, FDCA was the only bio-based platform compound included in the "Top 12 List of Value Added Chemicals" by the US Department of Energy since it has the potential to replace petrochemical monomers.[4] Indeed, one of its derivatives, the polyethylene 2,5-furandicarboxylate (PEF), is considered as the green alternative for polyethylene terephtha-late (PET); as a consequence, its industrial potential is very appealing and many companies have been involved in the investigation regarding this compound.[5]

Due to its abundant availability, lignocellulosic biomass (LCB) serves as a renewable and sustainable resource for the production of alternative biopolymers. LCB is primarily composed of cellulose (40–50%), hemicelluloses (20–40%) and lignin (20–30%).[6,7] Despite its robust structure, cellulose is preferably depolymerized to glucose, which can be then converted into various platform chemicals such as furan derivatives,[8] levulinic acid, lactic acid, formic acid, sorbitol, bio-alcohols, and biofuels.[9]

By converting LCB into monomers and subsequently conducting polymerization processes, it is possible to generate bio-based polymers. This approach offers a promising solution to a significant challenge associated with waste and pollution in the plastic industry.[10] As a matter of fact, the sugars production steps are initiated with delignification for lignin breakage and then the process is continued by hydrolysis;[11] the hemicellulose residue can be treated with different techniques such as autohydrolysis or dilute acid hydrolysis.[12] The obtained sugars, in the form of mono- and disaccharides, represent a useful feedstock for the production of versatile chemicals. For instance, hexose monosaccharides such as glucose and fructose can be catalytically dehydrated into 5-hydroxymethylfurfural (HMF). Hence, the hydrolysis of cellulose to glucose is usually followed by i) its isomerization to fructose, ii) fructose dehydration to produce HMF and finally the iii) HMF oxidation to obtain FDCA.[13]

All the chemical compounds taking part in the final step, including both the reagent (HMF) and the product (FDCA), as well as the intermediates, possess substantial industrial value. In particular, the 2,5-diformylfuran (DFF), 5-hydroxymethyl-2-fur-ancarboxylic acid (HMFCA), and 5-formyl-2-furancarboxylic acid (FFCA) intermediates are important biomass-derived compounds having wide-spread applications.[14] For instance, DFF can be used in the synthesis of ligands, pesticides, antifungal agents, fluorescent materials, and novel polymeric materials; HMFCA has been identified as an interleukin inhibitor with reported antitumoral activities; FFCA displays peculiar structural

[a] Dr. M. Bertini, Prof. Dr. F. Ferrante, L. Guercio, Dr. L. Lisuzzo, Prof. Dr. D. Duca
Dipartimento di Fisica e Chimica "Emilio Segrè",
Università degli Studi di Palermo,
Viale delle Scienze – 90128 Palermo, Italy
E-mail: francesco.ferrante@unipa.it

ChemCatChem

Research Article
doi.org/10.1002/cctc.202400179

Chemistry
Europe
European Chemical
Societies Publishing

properties which can be an advantage for the synthesis of drug derivatives.[15]

Extensive research has been conducted on the production of FDCA either in the past or recent years (an excellent review is the one by Zhang and Deng)[16] and identifying a suitable reaction in fact poses significant challenges. The direct oxidation of the HMF, which appears to be the most promising strategy for the synthesis of FDCA, can be obtained by using homogeneous as well as heterogeneous and bio-derived catalysts, or through electrochemical oxidation.[17] Since oxidizing agents play significant roles in HMF oxidation by facilitating the conversion on the catalyst surface, they have been thoroughly analyzed. The main agents used for the oxidation process are molecular oxygen, air, H_2O_2 and $KMnO_4$.[18] In particular, O_2 has been extensively studied due to its intrinsic oxidation ability, low cost, large availability, and eco-neutrality. Since bond breaking in O_2 has a high activation energy, supported noble metals like gold, palladium, platinum, ruthenium and rhodium have been comprehensively used as the main heterogeneous catalysts for the aerobic oxidation. H_2O_2 is also employed as an oxidant since it can provide a high active-oxygen content, it can be safely stored and its cost is affordable;[19] its efficiency in the oxidation of organic compounds, particularly when combined with gold or gold-alloy, has been established.[20–22] Even if homogeneous catalysis was also suggested, separation and recycling related issues make heterogeneous catalysis always more attractive, due to higher FDCA yield, easier separation and purification of FDCA and lower by-product yields.[23] In this context, catalysis based on noble metals, and among them gold in particular, plays a major role.[24–26]

Even if thermocatalytic conversion remains the dominant process for obtaining FDCA with the highest yields in commercially scalable applications,[27] electrochemical catalysis emerges as a viable alternative. Compared to traditional catalytic methods that rely on the control of reaction temperature or pressure, electrochemical catalysis has the advantage of depending on more easily adjustable factors, such as the electrode potential. Moreover, some innovative and cost-effective electrocatalysts demonstrated to have superior performances with respect to noble metals.[28] Exploring alternative approaches, the oxidation of HMF has been, as an example, investigated from a photocatalytic perspective, exemplified by the utilization of $ZnIn_2S_4$ nanoparticles. In this context, it was ascertained that the FDCA yield is not affected by the irradiation wavelength, even if the latter determines the formation of either the DFF or HMFCA intermediates.[29] Still, a different avenue for alcoholic group oxidation could involve photoelectrochemical approaches, as illustrated by the work of Terry et al., which used $BiVO_4$ films as photoelectrodes for benzyl alcohol oxydation.[30]

This multifaceted exploration underscores the different strategies employed in advancing the conversion of HMF towards FDCA production. However, despite the use of HMF as precursor is considered the most efficient method for obtaining FDCA, many challenges can arise due to the formation of various competitive compounds (humins, levulinic acid, etc).[31]

Moreover, the synthesis and extraction of HMF itself can be expensive and challenging to achieve. In view of this, adopting a one-pot strategy is becoming to be considered the most effective approach.[32]

In this work, halloysite nanotubes (HNTs) were considered as the support for the catalyst. Being natural nanoclays with low cytotoxicity,[33] HNTs offer versatility for various applications due to the possibility to be selectively functionalized depending on specific requirements.[34] The typical dimensions, polydispersity, and mineral purity of HNTs are influenced by their specific geological origin.[35] In particular, their length can vary from the submicron scale to 2–3 μm, the outer diameter from 15 to 200 nm whereas the inner diameter can range from 10 to 100 nm.[36] This kind of clay exhibits a hollow tubular structure, formed by aluminosilicate layers with a spiral-like morphology.[37] The surface chemistry of halloysite is very peculiar because of the differences between the inner and outer surfaces: the external surface is composed by the alternation of a tetrahedral Si—O based sheet overlapped to an octahedral Al—OH sheet.[38] Consequently, in the 2–8 pH range, the external silicon based surface is negatively charged and the inner aluminum based surface is positively charged.

The distinctive morphology of halloysite enables precise and selective modifications.[39] Functionalization of the positively charged inner surface can be achieved using molecules containing nucleophilic groups, while the modification of the negatively charged outer surface with electrophilic species (such as surfactants, polymers or biopolymers) can be accomplished through electrostatic interactions.[40] Furthermore, surface functionalization can be obtained through chemical covalent grafting using organosilanes.[41] These properties were exploited to use halloysite as catalytic support in the field of heterogeneous catalysis, building catalysts whose selectivity and efficiency can be improved upon decoration with noble metals.[42]

Even if HNTs and their modified variants are systems that can hardly be treated at the atomistic level by accurate computational studies, the design of suitable models[43,44] can give valuable insights on the structural and chemical characteristics of the inner and outer surfaces as well as on their interaction with adsorbed molecular systems.[45] Literature reported jointed experimental and computational investigations regarding the alkaline treatment of halloysite in order to create Si—OH groups at the external surface[46,47] and their further reactions with organosilanes, specifically (3-aminopropyl)-triethoxysilane (APTES).[48] It is worth noting that the silanization of the outer surface of halloysite is crucial for both industrial and catalytic purposes.[49] The termination of the silane chain can carry various functional groups, exhibiting a distinctive affinity towards metal atoms or enabling reactions with other compounds to form second-level functionalized systems, which could be particularly well-suited for the growth of metal nanoparticles. Therefore, in this work we focused on the use of gold-decorated outer HNT surface as catalyst for the conversion of HMF to FDCA using H_2O_2 as oxidizing agent. Herein, the adsorption of all the intermediates on the surface of APTES grafted HNTs bearing a gold atom as active site was considered

ChemCatChem

Research Article
doi.org/10.1002/cctc.202400179

Chemistry
Europe
European Chemical
Societies Publishing

in order to provide detailed atomistic insights about their geometrical and conformational properties, as well as on the energetics of the reaction path. Moreover, investigation is underway, both from computational and experimental perspectives, into the potential utilization of the acidic inner surface of halloysite nanotubes[42] for the dehydration reaction of fructose to produce HMF, a process known to be catalyzed by acidic environments.[13,50] In light of this, the present work would contribute to laying the groundwork for the development of a multifunctional catalytic system capable of facilitating a one-pot reaction from biomass-derived precursors to FDCA. Such a conversion would address current challenges associated with HMF separation, thereby consistently reducing costs and enhancing process efficiency.

Computational Methods

To perform the investigations reported in this work, several software tools were employed. The first ones, in procedural order, are NWPEsSe[51] and DFTB+.[52] The NWPEsSe code exploits the artificial bee colony algorithm[53] to identify the global minimum of a molecular system among all its possible geometric configurations. To do this, NWPEsSe generates a sequence of structures, whose geometry is determined by the information obtained on the previous ones, with the aim of finding new configurations that are increasingly closer to the global minimum. In order to accomplish this task, NWPEsSe must be interfaced to a computational chemistry software to gain knowledge on the energy associated with the molecular structures it generates, hence assessing how close the current guess is to the presumed global minimum. In the present work, NWPEsSe was interfaced to the DFTB+ code, which performs geometry optimizations at the self consistent charge density functional tight binding (SCC-DFTB) level of theory using the GFN2-xTB Hamiltonian recently proposed by Grimme.[54] In the optimization procedure, the catalyst part of the whole structure has been kept fixed, while there were no contraints on the organic species, which could thus adapt to its surroundings. This choice was made after also trying to generate by NWPEsSe a larger number of structures (10 thousand, specifically) without performing any DFTB geometry relaxation. The duration of the NWPEsSe calculations in the two cases was almost the same, but in this second scenario less stable structures were found with respect to the case in which a structure optimization was performed, meaning that the artificial bee colony algorithm alone is not able to compensate for the rigidity of the organic species in the search for the global energy minimum.

For each set of calculations (defined by the organic species and the catalytic system, the details of which will be explained in the following section), NWPEsSe was set to generate and optimize a number of structures ranging from 300 to 500. From each of these sets, geometries showing different adsorption modes on the catalytic system were selected, in order to refine them with two-layer ONIOM[55] calculations performed by means of the Gaussian 16 software.[56] When using this computational approach, one first has to select from the complete system (a.k.a. real system, in the ONIOM terminology) the sub-portion for which a better description is desired, known as the model system. Both high- and low-level calculations will therefore be performed on the model system, while only low-level calculations will be performed on the real system. Finally the extrapolated energy is considered. The fact that this latter is a simple sum of contributions, joined to the efficient way of treating link atoms in ONIOM, allows one to calculate with
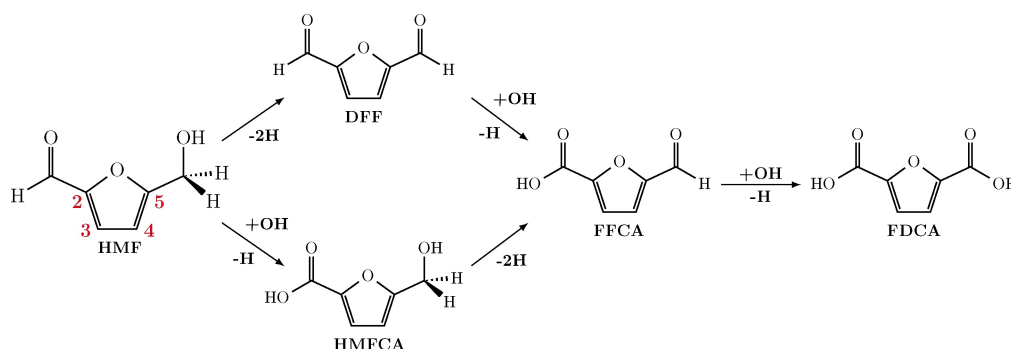
the same extrapolation method the molecular gradient for geometry optimization, and the molecular Hessian for vibrational frequency evaluation, hence the characterization of minima and transition states on the potential energy surface. The model system selected in the present work includes: i) the organic species present in the molecular aggregate (e.g. HMF); ii) the APTES chain along with the coordinated gold atom and iii) the portion of the halloysite silicon surface immediately underlying the APTES (also referred as "APTES base" in the following). Hydrogen atoms were used as links. The two chosen levels of theory were: i) for the high level, DFT with M06 exchange-correlation functional,[57] and cc-pVDZ basis set for all atomic nuclei except Au, for which cc-pVDZ-PP was used; ii) for the low level, molecular mechanics based on the universal force field (UFF). On the basis of several tests, we concluded that, for our systems, the exclusion of microiterations from the ONIOM optimization protocol stabilizes the convergence behavior of the algorithm, thus lowering the computational times, in a better way that the employment of coupled quadratic macro-step does. Further, in order to let the model system to feel the electronic influence from the remaining portion of the real system, the charge embedding scheme was used. All energy differences will be discussed in terms of ONIOM extrapolated energy including the vibrational zero-point energy; in order to take into account entropic contributions, mainly related to the intervention of small molecules along the reaction pathway, the thermodynamic of the HMF→FDCA conversion will be reported in terms of the calculated (standard conditions) Gibbs free energy variations.

Results and Discussion

Conformational Analysis

In the present study we considered the different chemical species appearing in the pathway from HMF to FDCA, as reported in the Scheme 1. All possible conformations of these species were investigated at the M06/cc-pVDZ level of theory. These conformations arise from the rotations of the side chains of the furan ring, and therefore their number varies depending on the type of functional groups and the molecular symmetry. This preliminary work had two purposes: i) identifying the most stable conformation, to be subsequently used to calculate the adsorption energies on the catalytic system; ii) providing a starting point for the subsequent study of adsorption structures by means of the NWPEsSe global optimizer.

Once this screening was concluded, it was possible to observe that, on average, there is a difference of 18 kJ mol^{-1} between the most stable conformation of a given species and the least stable one. At the extremes there are HMF, where this difference is only 6.2 kJ mol^{-1}, and FDCA, with a difference equal to 29.4 kJ mol^{-1}. Figure S1 in the supporting information shows in details the investigated conformations and their stability. Some considerations have to be made before proceeding with the actual investigation of the interaction modes with a given catalyst model. First, the energies we have discussed are relative to conformations in vacuum: it is likely that in solution, interactions with solvent molecules alter the energy gap between the most and the least stable configuration. For similar reasons, when considering the interaction with the catalytic system, it is not certain that the most stable

ChemCatChem

Research Article
doi.org/10.1002/cctc.202400179

Chemistry Europe
European Chemical
Societies Publishing

Scheme 1. Formal reaction scheme for the HMF to FDCA transformation, with the intermediate chemical species. Furanic ring carbon atoms numbering according to IUPAC is showed for HMF.

conformation of a given species is the one already arranged in the most appropriate way to interact with it. Consequently, we chose to proceed with the next step (the NWPEsSe calculations) using not necessarily the most stable conformation for each molecular species, but the one which, according to preliminary tests and chemical intuition, could be suitable to interact: in particular, we chose those conformations which show the oxygen nuclei of the functional groups on the same side as the furan ring oxygen. This choice proved to be hardly relevant on the final result, since the optimizations at the DFTB level themselves produced (during the exploration phase using NWPEsSe) many conformations that differ from the starting one, thus confirming that the investigated species possess a structure able to adapt to its surroundings.

Catalyst Model

The spiral supercell of a halloysite model, having an inner hole of about 1.5 nm and consisting of ca. 2000 atoms, was builded and relaxed by one of the authors some years ago.[43] By replicating this supercell a spiral nanotube can be generated, from which a portion of surface can be tailored and treated by accurate computational approaches.[44] This portion, which is the starting point for the construction of the catalyst model used in the present work, has $H_{48}Al_{24}Si_{24}O_{126}$ stoichiometry and is formed by a layer of SiO_4 tetrahedra superimposed to a layer of AlO_6 octahedra, which, maintaning the HNT curvature, mimick the outer and inner surfaces of the nanotube, respectively. It can be considered as a minimax model, in the sense that it is large enough to allow to investigate the adsorption of small molecules on the surface, or their chemical modifications, without significant border effects, but at the same time it is small enough to be treated by density functional theory.

By simulating the effect of alkaline conditions, the outer silicic surface was modified through the formation of surface silanol groups occurring after the insertion of water and OH^-.[47] Among all the structures that could be formed this way, namely as the second step of the present catalyst model generation, the configuration showing three $Si(OH)_3$ moieties protruding from the surface was chosen, as the product of the reaction of

the latter with 6 water molecules and 3 hydroxyl groups. This HNT fragment has three negative charges in the interlayer region but could exist (assuming reaction with further water molecules) also with partial or total charge neutralization.

In the third step, the modified HNT portion just described can be subjected to functionalization by means of a hydrolysis reaction with APTES, an organosilane of formula $NH_2(CH_2)_3Si(OCH_2CH_3)_3$, which reacts with the OH groups of the three surface silanols remaining attached after the elimination of three ethanol molecules.[48] The surface model now has an anchoring point, the $-NH_2$ group, for the coordination of a gold atom (its binding energy was estimated to be ca. 90 kJ mol^{-1} and the ground state of the whole system revealed to be in the doublet spin multiplicity), so creating the final catalyst model (CM-α) used in the present study and represented in Figure 1 along with the definition of the model system of the ONIOM procedure. The label α in the CM-α abbreviation will indicate the chemical form that the gold atom could assume along the reaction path (e.g. $\alpha = $ Au in the pristine catalyst model). In order to investigate the two limiting cases, both the charged catalyst and the neutral catalyst models were considered; they will be indicated as CC and NC, respectively, whatever is the actual form of Au in CM-α. The structural differences between the geometries of the two pristine CM—Au are minimal, and mainly concern one of the hydrogen bonds occurring between the silanol —OH groups and the surface, affected by the nature
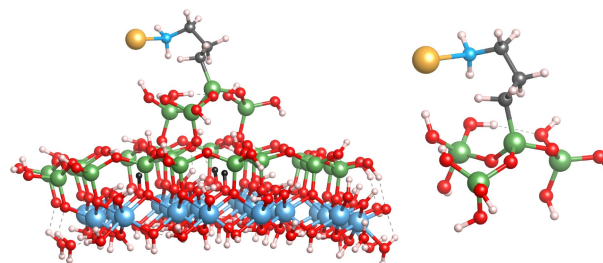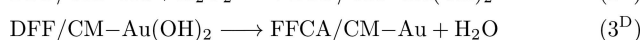

Figure 1. Modified halloysite structure functionalized with Au/APTES, used as catalyst model. On the left is shown the real system used in ONIOM calculations, whose model system definition is represented on the right. Atom colors code: H – white; C – gray; N – cyan; O – red; Al – light blue; Si – green; Au – yellow. The three black hydrogen centers between the Si-layer and Al-layer are present in the neutral system, while are absent in the charged one.

of the oxygen center (—O⁻ or —OH) in the interlayer. The surroundings of Au atom are essentially the same, i.e. the nitrogen atom at 2.39 Å and a non-bonded interaction with the H atom of the closest hydroxyl, at ca. 2.40 Å. Also, the overlap in the positions of the aminopropyl chain of APTES for the two cases is almost perfect, and the chain is slightly tilted towards the constellation of silanol groups due to a strong NH···OH hydrogen bond.
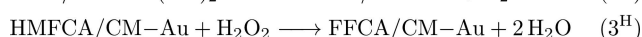
HMF to FDCA Conversion

In this work we postulated a series of reaction steps that would transform HMF to FDCA in the presence of hydrogen peroxide and the gold atom provided by the catalytic model. Accordingly, the reaction should proceed along with the steps reported in Scheme 2, where two different pathways are considered, one involving the diformylfuran as intermediate

D-path

$$\text{HMF/CM}-\text{Au} + \text{H}_2\text{O}_2 \longrightarrow \text{DFF/CM}-\text{Au} + 2\,\text{H}_2\text{O} \qquad (1^\text{D})$$

$$\text{DFF/CM}-\text{Au} + \text{H}_2\text{O}_2 \longrightarrow \text{DFF/CM}-\text{Au(OH)}_2 \qquad (2^\text{D})$$

$$\text{DFF/CM}-\text{Au(OH)}_2 \longrightarrow \text{FFCA/CM}-\text{Au} + \text{H}_2\text{O} \qquad (3^\text{D})$$

H-path

$$\text{HMF/CM}-\text{Au} + \text{H}_2\text{O}_2 \longrightarrow \text{HMF/CM}-\text{Au(OH)}_2 \qquad (1^\text{H})$$

$$\text{HMF/CM}-\text{Au(OH)}_2 \longrightarrow \text{HMFCA/CM}-\text{Au} + \text{H}_2\text{O} \qquad (2^\text{H})$$

$$\text{HMFCA/CM}-\text{Au} + \text{H}_2\text{O}_2 \longrightarrow \text{FFCA/CM}-\text{Au} + 2\,\text{H}_2\text{O} \qquad (3^\text{H})$$

Common to both

$$\text{FFCA/CM}-\text{Au} + \text{H}_2\text{O}_2 \longrightarrow \text{FFCA/CM}-\text{Au(OH)}_2 \qquad (4)$$

$$\text{FFCA/CM}-\text{Au(OH)}_2 \longrightarrow \text{FDCA/CM}-\text{Au} + \text{H}_2\text{O} \qquad (5)$$

Net process

$$\text{HMF} + 3\,\text{H}_2\text{O}_2 \longrightarrow \text{FDCA} + 4\,\text{H}_2\text{O}$$

Scheme 2. The postulated steps in the conversion of HMF to FDCA by means of H₂O₂ and the gold functionalized HNT catalyst model.

(D-path), the other one passing through the 5-hydroxymethyl-2-furancarboxylic acid species (H-path).

In the following, a description of the main interaction modes for all the involved organic species with both the neutral and charged catalytic system is given, in the order they appear in Scheme 2. Considering the different organic species involved and the multiple catalyst arrangements (that are different for the charge and the gold ligands), there are a total of 16 sets of systems. Thus, since the total number of investigated structures is 305, 19 configurations on average were considered for each organic species/CM pair. While the relative energies of all the configurations occurring in the investigated sets are reported in Tables S1–S10 of Supporting Information, Figures 2 and 3 show the lowest energy geometries for the systems formed by the main species along the HMF→FDCA conversion path adsorbed on the pristine CM—Au, in the neutral and charged form, respectively. In the following paragraph the most important system configurations are described, their energies being reported with respect to the energy of the most stable structure in the given set. Given the nature of the HNT functionalized surface, bearing a large number of interaction sites, we believe it is correct to state that it is not possible to exclude a priori the existence of configurations of equal stability, or even more stable, other than those reported in this investigation.

HMF/CM—Au

The most stable configuration of HMF in the NC model (Figure 2a) features an Au—C5 interaction and a intricate network of hydrogen bonds between HMF and the silanolic hydroxyl groups of the APTES-base (which in the following will be collectively indicated as SOG), where the oxygen atom of the alcoholic moiety acts both as H-bond donor and acceptor, while the furanic and carbonyl oxygen atoms act as acceptors. At $+39.0\,\text{kJ}\,\text{mol}^{-1}$ of energy there is a variation of the adsorption
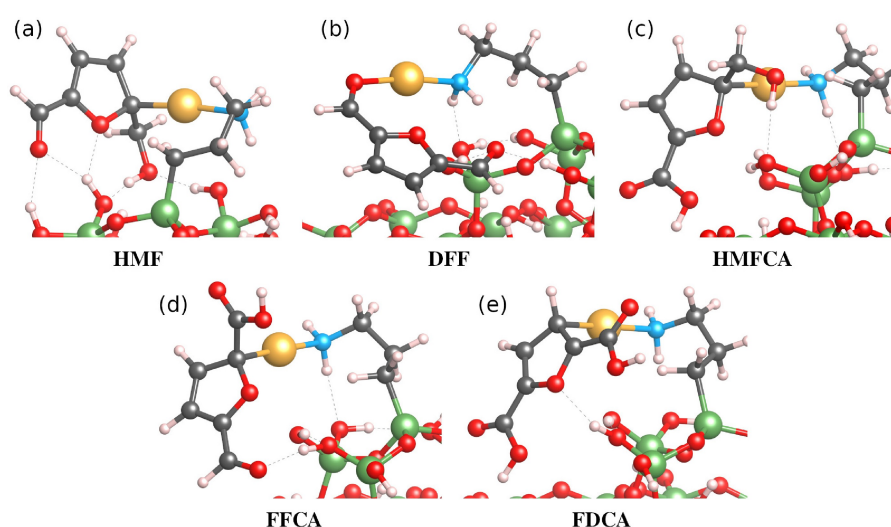

Figure 2. Best adsorption configurations of the main molecular species along the path for the HMF to FDCA on the neutral catalytic system, found by the NWPEsSe/ONIOM-based computational protocol. For the sake of clarity, only the relevant portion of the catalyst is shown. Atom colors: H – white; C – gray; N – cyan; O – red; Si – green; Au – yellow.
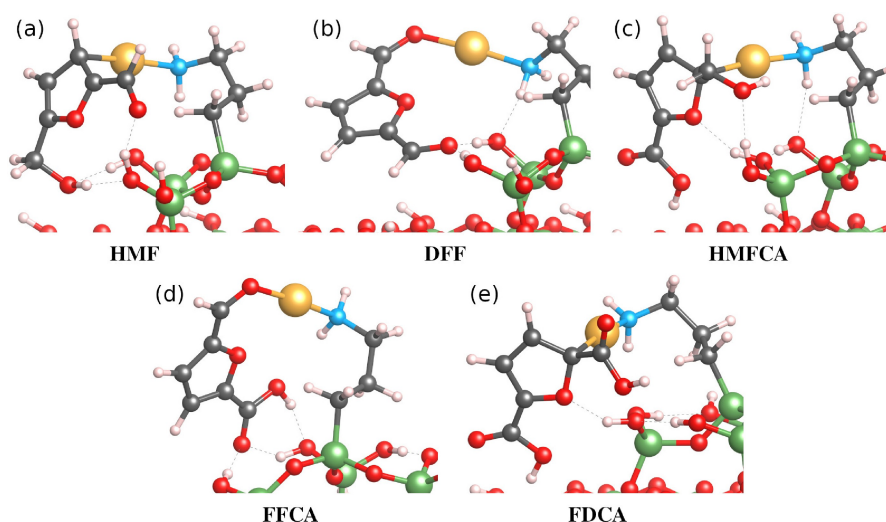
ChemCatChem

Research Article
doi.org/10.1002/cctc.202400179

**Chemistry
Europe**
European Chemical
Societies Publishing

Figure 3. Best adsorption configurations of the main molecular species along the path for the HMF to FDCA conversion on the charged catalytic system, found by the NWPEsSe/ONIOM-based computational protocol. For the sake of clarity, only the relevant portion of the catalyst is shown. Atom colors: H – white; C – gray; N – cyan; O – red; Si – green; Au – yellow.

mode, and the Au–C3 interaction becomes effective. The first structure showing Au–O(carbonyl) interaction occurs at an energy of $+53.1\ kJ\,mol^{-1}$, while at $+72.2\ kJ\,mol^{-1}$ the interaction between Au and C(carbonyl) begins to appear. The furanic oxygen atom shows an interaction with the amino group in a configuration which is at ca. $120\ kJ\,mol^{-1}$ in the energy scale, while up to $130\ kJ\,mol^{-1}$ no adsorption modes involving gold and other atomic centers of HMF were revealed. Instead, it is worth to note that in a number of structures generated by NWPEsSe the migration of a hydrogen atom from the $-CH_2-$ group of HMF to Au occurred, thus leaving a DFF species hydrogenated in the aldehyde oxygen atom (HDFF/CM-AuH). After the subsequent ONIOM optimization, the most stable HDFF interaction mode resulted only $10.8\ kJ\,mol^{-1}$ less stable than the favored HMF adsorption configuration. The analysis of spin density in this structure reveals a thickening of α-electrons (whose two lobes shape is perpendicular to the plane of the furanic ring) centered on the deprived carbon, i.e., to put it less correctly but more incisively, the unpaired electron is most likely to be found in the surroundings of the aforementioned carbon.

Using the CC model, on the other hand, a significantly different scenario was found. Even if the same variety of interaction modes described for neutral systems is maintained, in this case the most stable HMF adsorption geometry is the one featuring Au–C3 interaction, joined to several HMF-SOG hydrogen bonds (with the exclusion of the furanic oxygen atom, Figure 3a) and followed, from $+26$ to $+60\ kJ\,mol^{-1}$, by configurations showing the Au–O(carbonyl) feature. The first mode with Au–C5 interaction is at $68.1\ kJ\,mol^{-1}$ and the first one involving Au–C(carbonyl) is at $106.9\ kJ\,mol^{-1}$. Also in the charged case the HDFF intermediate was found, but in a high $(+63.5\ kJ\,mol^{-1})$ energy configuration.

Assuming that the gold atom is the active site of the catalytic process, we are allowed to think that a certain

transformation of a part of the HMF molecule would occur if that part is inside the gold interaction region. Therefore, it is reasonable to hypothesize that the HMF adsorption mode involving the Au–C5 interaction, preferably occuring in NC, would trigger the D-path, not to mention the fact that the HDFF intermediate, which would appear in-between the (1^D) step of Scheme 2.

$$HMF/CM-Au \rightarrow HDFF/CM-AuH \qquad (1)$$

$$HDFF/CM-AuH + H_2O_2 \rightarrow DFF/CM-Au + 2H_2O \qquad (2)$$
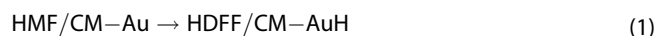
is obtained as a low energy species already at the level of geometry optimization. Conversely, the preference for the Au–C3 interaction in CC would geometrically lead firstly to the transformation of the HMF aldehydic group, which is what occurs in the H-path. To investigate from the kinetic point of view the HMF→HMFCA conversion the thorough study of H_2O_2 fragmentation on gold would be needed, which would lead too far from the aims of preliminary nature of the present work. However, some considerations can be made in this regard. According to the computational method used in this work, the fragmentation of H_2O_2 to 2OH on CM–Au is a largely exergonic reaction, (standard ΔG of nearly $-200\ kJ\,mol^{-1}$ at $T=298$ K). This is in agreement with literature data, such as those of Li et al.,[58] claiming the presence of OH radicals to explain the enhanced chemiluminescence of the luminol/H_2O_2 system coupled with a Au/Ag alloys, and those of Lin et al.,[59] which investigated the same decomposition here presented but on iron oxides. In particular, in view of the exergonicity above, it is possible to hypothesize that what is suggested in the work of Lin et al. could happen also on CM–Au: the preferred H_2O_2 decomposition route gives ·H and ·OOH but the thermodynamic instability of the peroxy radical, joined to the fact that the fragmentation occurs in a restricted space, instantaneously

ChemCatChem

Research Article
doi.org/10.1002/cctc.202400179

Chemistry Europe
European Chemical
Societies Publishing

convert ·H and ·OOH to two ·OH radicals that, according to thermodynamics, will never go backwards to form the H_2O_2 molecule. In conclusion, we could infer that the fragmentation of H_2O_2 to 2OH on CM—Au is driven to a good extent by thermodynamics.

The migration kinetic of a hydrogen atom, on the other hand, does not involve other species or long reaction pathways, so we report here the results obtained for the HMF→HDFF step, and later the corresponding ones for the dehydrogenation of HMFCA on the way to FFCA. The energetics of the HDFF formation elementary step is reported in Figure 4, which shows a calculated energy barrier of 99.3 kJ mol^{-1} for the hydrogen migration. It is to emphasize that the reactive configuration of the HMF is not necessarily the most stable one, and the same can be said for the HDFF product. Actually, in the present case, the HMF/CM—Au reagent is a high energy structure ($+63.0$ kJ mol^{-1} in the relative energy scale) and, by applying the calculation protocol used in this work on the various interaction modes of HDFF, we observed that also this species adopts a high energy configuration (i.e. $+39.9$ kJ mol^{-1} with respect to the most stable one; see Table S11). However, as already said, the difference between the most stable geometries of HMF and HDFF is only 10.8 kJ mol^{-1}, which would be the net energy expense for the elementary step when considering the rearrangement of both species on the surface, an amount of energy that will be easily recovered in the next steps along the pathway.

DFF/CM—Au

The most stable adsorption of DFF on NC, shown in Figure 2b, involves both of its carbonyl groups, one of which is employed in the interaction with gold, the other in hydrogen bonds with the amino group of APTES and SOG. Up to 65 kJ mol^{-1}, our computational protocol identified configurations showing only
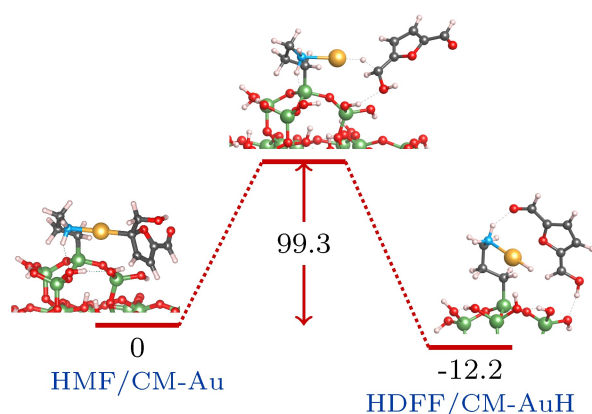

Figure 4. The species and energies involved in the elementary process trasforming HMF to HDFF, by a hydrogen atom migration towards the gold atom. The reaction energy and the energy barrier are reported, in kJ mol^{-1}, in terms of energy differences including vibrational zero-point contribution; the corresponding values in terms of standard free enegy differences are -11.9 and 90.7 kJ mol^{-1}, respectively. Atom colors: H – white; C – gray; N – cyan; O – red; Si – green; Au – yellow.

Au—O(carbonyl) as main interaction, with Au—C3 and Au—C2 appearing only at $+79.4$ and $+83.0$ kJ mol^{-1}, respectively. Even with the charged catalyst something similar is observed, i.e. being the Au—O interaction, together with various hydrogen bonds with the surrounding SOG, the preferred mode up to $+85$ kJ mol^{-1} (Figure 3b). It was found that the Au—C3 and Au—C2 interactions occur in structures at $+86.0$ and $+91.7$ kJ mol^{-1} from the most stable, respectively, after which there are very high energy adsorption modes where the gold atom is not involved.

DFF/CM—Au(OH)₂

This species should appear as a product of the hydrogen peroxide fragmentation on the gold atom, needed to convert DFF to FFCA (steps 2^D and 3^D). The variety of interactions found in this set of calculations performed on NC is rather limited, presumably due to the clutter around the gold atom. The most stable structure, depicted in Figure S2a in the supporting information, features a hydrogen bond between DFF and one of the hydroxyl group coordinated to Au. At very close energy ($+2.8$ kJ mol^{-1}) there is a conformation in which DFF interacts with the alkyl chain of APTES, and yet another at $+12.9$ kJ mol^{-1} in which one of the carbonyl groups is close to the APTES amino group. In no case interactions of Au—C kind were observed. Similarly, also in CC the most stable structure shows the interaction between the carbonyl group of DFF and an Au-coordinating hydroxyl group (Figure S2d). The next two structures in order of stability show one DFF-SOG hydrogen bond ($+16.7$ kJ mol^{-1}) and an interaction between DFF and the APTES chain ($+17.0$ kJ mol^{-1}). Again, no direct Au—C interaction was found.

FFCA/CM—Au

Regarding this series of calculations, all possible interactions between the FFCA species and Au atom were found on NC, except Au—C(carboxyl). In the most stable structure, shown in Figure 2d, there is an Au—C2 interaction and one hydrogen bond between the aldehydic O atom and SOG. In order of strength, the following are the other observed interactions with FFCA carbons: Au—C3 ($+31.9$ kJ mol^{-1}), Au—C4 ($+44.0$ kJ mol^{-1}), Au—C5 ($+65.5$ kJ mol^{-1}), and Au—C(carbonyl) ($+82.9$ kJ mol^{-1}). It is clear that these are extremely disfavored compared to the Au—C2 interaction, but there is also a structure at $+8.5$ kJ mol^{-1} that features an Au—O(carbonyl) interaction and a hydrogen bond with SOG. As a final note, a structure is found in which Au strips the hydrogen from C(carbonyl), but this conformation is highly unstable, at $+149.2$ kJ mol^{-1} in the energy scale. On the other hand, on CC the preferred configuration (Figure 3d) shows an Au—O(carbonyl) interaction plus an FFCA-SOG hydrogen bonds net involving the carboxylic group. In an energy range extending up to $+12.5$ kJ mol^{-1} from the most stable, we find a number of structures that exhibit the same interaction with gold but vary in the position and geometry of the

ChemCatChem

Research Article
doi.org/10.1002/cctc.202400179

**Chemistry
Europe**
European Chemical
Societies Publishing

hydrogen bond. Structures that present an interaction between gold and a carbon of the furanic ring are higher in energy: Au–C2 ($+15.0$ kJ mol^{-1}), Au–C3 ($+24.4$ kJ mol^{-1}), Au–C4 ($+47.0$ kJ mol^{-1}), and Au–C5 ($+50.6$ kJ mol^{-1}).

HMF/CM–Au(OH)$_2$

While the D-path could be triggered directly from the pristine CM–Au, in order to produce HMFCA by the 2^H step, the HMF species has to be on a catalyst form where H$_2$O$_2$ is already fragmented to two –OH groups on the gold atom (steps 1^H).

When the NC is considered, the most stable structure of the HMF/CM–Au(OH)$_2$ species (Figure S2b) shows the hydroxyl group of HMF donating a hydrogen bond to an Au-coordinating –OH group, while at the same time it is accepting one from a SOG. The next most stable structure is found at $+39.5$ kJ mol^{-1}, and in this case it is the carbonyl group that receives a hydrogen bond from –Au(OH)$_2$. Other configurations differ essentially for the arrangement of hydrogen bonds interactions.

Several interesting things were found in the most stable structure of the series of calculation on CC: each of the Au-coordinating hydroxyl groups donates a single hydrogen bond, one to O(carbonyl), the other to O(hydroxyl) of HMF, the latter being also involved in a hydrogen bond with SOG (see Figure S2e). This structure with a very intricate H-bond network is closely followed ($+4.6$ kJ mol^{-1}) by another one in which the only interactions occur with SOG: to be more specific, both functional groups of HMF are involved in two hydrogen bonds with the same silanolic hydroxyl group.

HMFCA/CM–Au

Using the most stable conformation of HMFCA as a starting point for the NWPEsSe/ONIOM investigation, it was found that the preferred adsorption configuration on NC (its geometry is depicted in Figure 2c) is the one exhibiting one Au–C5 interaction and one hydrogen bond with a SOG where the hydroxyl group acts as donor. It is, however, essentially isoenergetic with a configuration where the Au–C3 interaction occurs and the HMFCA adopted a conformation where both the carboxylic and the hydroxymethyl groups are rotated with respect to the most stable one. At $+26.6$ kJ mol^{-1} there is the first structure that presents the Au–C2 interaction. This had never been observed in the case of HMF and DFF. The carboxylic oxygen is involved in interactions with gold only at energy higher than $+90$ kJ mol^{-1}. It is worth noting that several HFFCA/CM–AuH structures were also found, where, as happened in the case of HMF to HDFF, there was the hydrogen shift from –CH$_2$– to the gold atom; remarkably, the most stable of these structures is also the most stable configuration at all, being -31.7 kJ mol^{-1} in the energy scale referred to minimum energy of the HMFCA/CM–Au geometry (for the analysis of HFFCA configurations see Table S12). Since the HFFCA species could be preliminar to the formation of FFCA in the H path, also in this case the transition state for the migration of hydrogen

towards gold was calculated. The energy barrier of 91.5 kJ mol^{-1} and the reaction energy of -11.5 kJ mol^{-1} (79.9 and -14.8 kJ mol^{-1}, respectively, in terms of standard free energies) are pretty similar to those found for the HMF-HDFF conversion. This is not surprising since the protagonists of the two elementary stages show structures that differ only in functional groups far from the reactive portion.

The best adsorption conformation presents the Au–C5 interaction also in the CC model, as well as HMFCA-SOG hydrogen bonds involving, as acceptors, the hydroxyl and furanic O atoms; the geometry is reported in Figure 3c. The first structure with Au–C2 or Au–C3 interactions are almost at the same level, at ca. $+40$ and $+50$ kJ mol^{-1}, respectively. As a matter of fact, there are a number of low energy adsorption modes where only hydrogen bonds with the HNT silicic surface are formed and there is not a specific interaction with the gold center. The Au–C(carboxyl) is at energy higher than $+70$ kJ mol^{-1}. Besides the case where hydrogen migration from HMFCA to Au produces the HFFCA species ($+38.6$ kJ mol^{-1}), among the most exotic structures found in this series there are some in which Au strips the acidic hydrogen ($+77.6$ kJ mol^{-1}), or even the alcoholic hydrogen (this is the unique case in all the calculations done in this work), while, being at $+156.6$ kJ mol^{-1}, this is certainly not a favored case.

FFCA/CM–Au(OH)$_2$

This species is involved in the common part of the D and H pathways (steps 4 and 5 of Scheme 2) and, since FFCA is formed on the pristine catalyst, the H$_2$O$_2$ fragmentation should occur in the presence of FFCA (this is just the same situation encountered in the conversion of DFF). On the NC system, the most stable structure (Figure S2c) is the one in which the carboxyl group of FFCA creates a network of hydrogen bonds with hydroxyl groups of both silanols and gold. Different configurations were found: in some of them there is the simple FFCA-SOG hydrogen interaction ($+6.0$ kJ mol^{-1}), in others the FFCA molecule is close to the gold and the amino group of APTES ($+15.5$ kJ mol^{-1}). However, the very peculiar structure is the one (fairly high in energy, $+61.1$ kJ mol^{-1}) in which FFCA strips an –OH group from Au, binding it to the carboxyl carbon and thus forming a gem-diol. In this structure, the original oxygen of the carboxyl group (the one lacking hydrogen) is bonded to gold in according to a linear N–Au–O geometry. Also in the case of CC the most favorable interaction between FFCA and catalyst occurs with the formation of a hydrogen bond between carboxyl oxygen and one Au-coordinating –OH group, and another one between FFCA and SOG (Figure S2f). In addition to the other fairly standard modes of interaction in which FFCA stands close to the APTES chain, there is a conformation at $+46.8$ kJ mol^{-1} in which Au interacts with the carboxyl oxygen, creating a square planar coordination around the metal center, which was not found in the set of calculations related to the neutral catalyst.

ChemCatChem

Research Article
doi.org/10.1002/cctc.202400179

Chemistry
Europe

European Chemical
Societies Publishing

FDCA/CM–Au

Due to the molecular symmetry of FDCA, there are fewer possible interaction modes with the catalyst: the favored configuration on NC shows the Au–C3 interaction and one hydrogen bond involving the furanic oxygen (Figure 2e), followed at $+5.2$ kJ mol^{-1} by a structure with Au–C2 interaction and at $+12.6$ kJ mol^{-1} by another form where FDCA interacts with SOG exclusively by means of hydrogen bonds. It is worth to note that all these configurations fall within a very narrow energy range. Finally, in the case of CC, calculations revealed that the most stable adsorption geometry (Figure 3e) features the Au–C2 interaction, with a position of FDCA that however closely resembles the one adopted in the neutral catalyst form. Interestingly, structures that show the Au–C3 interaction cannot be found up to $+45.7$ kJ mol^{-1} of energy. Among others, a significant configuration was found at $+37.3$ kJ mol^{-1} in which the two carboxyl groups form as many hydrogen bonds with the amino group of APTES.

Adsorption and Reaction Energetics

Table 1 summarizes the results discussed above for each set of calculated systems, togeteher with a brief description of the presumably stronger contribution to the interaction between the organic species and the catalyst model. In order to give a reliable evaluation of the interaction energies, calculation of the basis set superposition error (BSSE) was performed by means of the counterpoise approach as implemented in Gaussian 16. Since, at present, the use of this method along with ONIOM calculations is not an option, in order to estimate BSSEs we did not consider the whole structure but just the model system, on which the counterpoise scheme was applied at DFT-M06 level. It is to note that the one employed is an approximated approach which is acceptable considering that we are only in

search of a crude estimation of an error. However, having such a guess could be important given the variety of organic species involved and the different nature of their interactions with the catalysts. The electronic adsorption energies, reported in Table 2, are calculated with respect to the generic reaction S + CM-Au→S/CM-Au (where S is the organic species involved), using the formula $\Delta E_{ads} = E_{S/CM-Au} - E_S - E_{CM-Au}$, being E_S the energy of the most stable conformation in vacuum.

All the lowest energy adsorption configurations show an interaction between a carbon of the furanic ring and the gold atom, with the exception of DFF (in both NC and CC) and FFCA (in CC) which instead preferably interact with the metal center via the carbonyl oxygen. As a matter of fact, the adsorption energy values suggest that DFF is the species that most strongly interacts with the catalytic fragments, in both neutral and charged cases. This is somewhat surprising, since Au does usually not show special affinity to oxygen. However, a closer look at the adsorption geometry of DFF on NC reveals one hydrogen bond with the amino group and three hydrogen bonds with SOG (see Figure 2b), two of which, present also in the CC model, are unusually short (ca. 1.7 Å) with respect to the distances that were generally found in the here investigated systems (e.g., the distances in the similar H-bond geometry occurring in HMF/CM–Au are ca. 2 Å). The high interaction energy of DFF could be therefore temptatively explained by considering its unique ability to delocalize electrons in its highly symmetric structure, which in this particular case would give a partial radical character to the carbonyl oxygen that does not interact with gold.

FFCA-charged catalyst fragment, on the other hand, has the lowest adsorption energy, and although in the related set of calculations some configurations where gold and carbon interact have been found, their lower stability can in no case be attributed to missing hydrogen bonds, which are indeed always

Table 1. Relevant interaction mode found in the most stable adsorption configuration of each organic species/catalytic system pair.

Species[a]	Neutral model[b]	Charged model[b]
HMF/CM–Au	Au–C5	Au–C3
HDFF/CM–AuH	HDFF···SOG	HDFF···NH₂
DFF/CM–Au	Au–O(carbonyl)	Au–O(carbonyl)
HMFCA/CM–Au	Au–C5	Au–C5
HFFCA/CM–AuH	HFFCA···SOG	HFFCA···SOG
FFCA/CM–Au	Au–C2	Au–O(carbonyl)
FDCA/CM–Au	Au–C3	Au–C2
HMF/CM–Au(OH)₂	AuOH···O(hydroxyl)	AuOH···O(carbonyl)
DFF/CM–Au(OH)₂	AuOH···O(carbonyl)	AuOH···O(carbonyl)
FFCA/CM–Au(OH)₂	AuOH···O(carboxyl)	AuOH···O(carboxyl)

[a] The preferred interaction mode of the HDFF and HFFCA intermediate species with the corresponding form of the catalyst are also considered. [b] Solid line (–) is used for interaction other than hydrogen bonds, for which a dotted line (···) is employed.

Table 2. Adsorption energy (ΔE_{ads}), guess for the BSSE, and corrected adsorption energy ($\Delta \bar{E}_{ads}$) for various species interacting with neutral (NC) and charged catalyst model (CC).

Species	ΔE_{ads}[a]	BSSE[b]	$\Delta \bar{E}_{ads}$[c]
	kJ mol^{-1}		
HMF/CM–Au (NC)	−185.4	43.7	−141.7
DFF/CM–Au (NC)	−194.7	43.3	−151.4
HMFCA/CM–Au (NC)	−141.2	34.8	−106.4
FFCA/CM–Au (NC)	−165.7	26.2	−139.5
FDCA/CM–Au (NC)	−127.3	28.0	−99.3
HMF/CM–Au (CC)	−169.7	43.2	−126.5
DFF/CM–Au (CC)	−200.5	40.5	−160.0
HMFCA/CM–Au (CC)	−169.0	34.2	−134.8
FFCA/CM–Au (CC)	−154.4	61.9	−92.5
FDCA/CM–Au (CC)	−137.0	29.0	−108.0

[a] ΔE_{ads} are computed using the ONIOM extrapolated energy corrected for the zero point vibrational energy. [b] The BSSE values obtained from the computations on the sole model systems are used. [c] $\Delta \bar{E}_{ads} = \Delta E_{ads} +$ BSSE.

ChemCatChem

Research Article
doi.org/10.1002/cctc.202400179

Chemistry
Europe
European Chemical
Societies Publishing

present. The large BSSE correction conversely can be explained quite easily by noting that the carboxyl group of FFCA faces towards the APTES base, with which it makes many hydrogen bonds, whereas in the case of the neutral system it is facing upwards and its participation in the interaction with the catalyst is quite limited. Even if the case of FFCA on CC is worth to be further explored, the trend reported in Table 2 loosely suggests that the presence of the carboxyl group in the organic species lowers the interaction energy and, after all, indicates that the desorption energy of the final FDCA product is lower (on NC in particular) than the adsorption energy of the HMF starting reagent, an issue which is surely helpful for the success of the conversion.

Finally, taking a look at the Gibbs free energy variations calculated for the reaction steps of Scheme 2 and collected in Table 3, it can be concluded that both the individual and the net processes are characterized by a marked exergonicity. In particular, there are no sensible differences between the energy values obtained in the two catalytic models. Another similarity concerns the 1^D and 3^H steps, where the reacting organic species loses a total of two hydrogen atoms, which have a comparable ΔG (ca. -300 kJ mol^{-1}). The 2^D, 3^D, 1^H, and 2^H steps finally deserve a more in-depth comment. The 2^D and 1^H reactions concern the fragmentation of a hydrogen peroxide molecule on the catalyst, differing in the organic species adsorbed. In steps 3^D and 2^H, conversely, the reacting organic species acquires a hydroxyl group. Considering the ΔG relative to the neutral catalyst, it is clear that the energetic trend of these two processes (peroxide fragmentation and hydroxyl acquisition) are inverted: in the D-path the 3^D process in which FFCA is formed is indeed favored, while in the H-path is more exergonic the dissociation of hydrogen peroxide, rather than the acquisition of a hydroxyl by HMF. A similar, but less accentuated, trend is also found in the charged catalyst. Interestingly, this aspect could be plainly traced back to the already described difference between the interaction modes of the HMF/HMFCA and DFF/FFCA pairs.

Table 3. Standard reaction free energies calculated for the steps reported in Scheme 2 on both neutral, ΔG_{NC}, and charged catalyst, ΔG_{CC}.

Step	ΔG_{NC}/kJ mol^{-1}	ΔG_{CC}/kJ mol^{-1}
1^D	−309.2	−332.8
2^D	−119.3	−140.9
3^D	−211.2	−168.4
1^H	−201.6	−194.2
2^H	−107.2	−155.4
3^H	−330.9	−292.4
4	−181.3	−215.2
5	−133.5	−127.0
net	−954.5	−984.3

Conclusions

Optimizing the synthesis of 2,5-furandicarboxylic acid (FDCA), along with other intermediates, from 5-hydroxymethylfurfural (HMF) stands out as a particularly promising step in the chemical valorization of biomass.

In the computational investigation presented in this article, framed as a research perspective, the use of a specifically functionalized halloysite nanotube is explored. This model features a gold atom attached to the amino group of a (3-aminopropyl)triethoxysilane residue embedded on the silicic surface, which is employed as a catalyst for the oxydation of HMF in the presence of hydrogen peroxide. This in view to propose a one-pot reactor where the acid environment of the inner surface of the nanotube would act as catalyst for the dehydration of fructose to form HMF, while the modified and functionalized outer surface would convert the hardly isolable HMF molecule to valuable products.

It is recognized that substantial efforts are needed just to design the corresponding experimental approach based on the findings of the presented computational model. With respect to this, one of the major challenge to face would be the growth of gold in large clusters or nanoparticles, which could reveal an undesired issue, given the use of a noble, expensive metal. Even if halloysite silicic surface modification has reached considerable sophistication, there is still a long way to go before a precise atomistic creation of a surface-functionalized nanotube is achieved. On the other hand, if gold on the HNT surface would be prevented from aggregation, the described process could be considered as a borderline example between heterogenous and homogenous catalysis, being gold the small active center and the silicic HNT surface a portion of space where reactants and intermediates could be adsorbed and addressed to react.

From the computational side, conversely, the following issues must be solved for a more instructive and useful knowledge of the process: i) the calculation of the reaction mechanisms (i.e. the characterization of the involved transition states and corresponding energy barriers) must be undertaken; ii) the intervention of H$_2$O$_2$, which should have the double role of being an active reactant and restoring the catalitic center, must be detailed at the atomistic level; iii) at least micro-solvation should be considered, in order, e.g., to evaluate energy differences between the various interaction modes that take into account also the reorganization of the solvent molecules; iv) the catalytic properties of small gold clusters, most likely to form if a certain population of functionalization is present on the surface, are worth to be investigated. Never-theless, the present investigation gives some hints that, in our opinion, make the conversion of HMF on gold-functionalized HNT worth to be further investigated. Indeed, i) all the considered reaction intermediates well interact with the catalyst model, in particular in the catalytic active region, ii) all the analyzed processes, including H$_2$O$_2$ fragmentation on the pristine catalyst, are largely exergonic and the standard free energy variation for the whole process is calculated to be nearly −1 MJ mol^{-1}; iii) computational results highlight the natural

ChemCatChem

Research Article
doi.org/10.1002/cctc.202400179

**Chemistry
Europe**
European Chemical
Societies Publishing

activity of gold to subtract hydrogens from some species, specifically that of the $-CH_2-$ group of hydroxymethylfurfural, a step that could trigger a process which would continue in a radicalic way; iv) the amount of negative charge on the HNT silicic outer surface can force the organic species to adopt geometric configurations that could lead to discriminate the preferred route between the two different branches of the conversion reaction.

Acknowledgements

Conflict of Interests

The authors declare that they have no known competing financial interests or personal relationships that could have appeared to influence the work reported in this paper.

Data Availability Statement

The data that support the findings of this study are available from the corresponding author upon reasonable request.

[1] S. Sadjadi, N. Abedian-Dehaghani, X. Zhong, M. M. Heravi, P. Yuan, *Appl. Clay Sci.* **2023**, *237*, 106896.
[2] M. Sajid, X. Zhao, D. Liu, *Green Chem.* **2018**, *20*, 5427–5453.
[3] T. Su, D. Zhao, Y. Wang, H. Lü, R. S. Varma, C. Len, *ChemSusChem* **2021**, *14*, 266–280.
[4] K. Loos, R. Zhang, I. Pereira, B. Agostinho, H. Hu, D. Maniar, N. Sbirrazzuoli, A. J. Silvestre, N. Guigo, A. F. Sousa, *Front. Chem.* **2020**, *8*, 585.
[5] N. van Strien, J. Niskanen, A. Berghuis, H. Pöhler, S. Rautiainen, *ChemSusChem* **2024**, *17*, e202300732.
[6] M. Lara-Serrano, S. Morales-delaRosa, J. M. Campos-Martín, J. L. Fierro, *Green Chem.* **2020**, *22*, 3860–3866.
[7] H. Kobayashi, A. Fukuoka, *Green Chem.* **2013**, *15*, 1740–1763.
[8] W. Li, T. Zhang, H. Xin, M. Su, L. Ma, H. Jameel, H.-m. Chang, G. Pei, *RSC Adv.* **2017**, *7*, 27682–27688.
[9] X. Cui, X. Zhao, D. Liu, *Green Chem.* **2018**, *20*, 2018–2026.
[10] Z. Zhang, G. W. Huber, *Chem. Soc. Rev.* **2018**, *47*, 1351–1390.
[11] Y. Sun, J. Cheng, *Bioresour. Technol.* **2002**, *83*, 1–11.
[12] D. Tocco, C. Carucci, M. Monduzzi, A. Salis, E. Sanjust, *ACS Sustainable Chem. Eng.* **2021**, *9*, 2412–2432.
[13] C.-T. Chen, C. V. Nguyen, Z.-Y. Wang, Y. Bando, Y. Yamauchi, M. T. S. Bazziz, A. Fatehmulla, W. A. Farooq, T. Yoshikawa, T. Masuda, K. C. W. Wu, *ChemCatChem* **2018**, *10*, 361–365.
[14] D. Zhao, T. Su, Y. Wang, R. S. Varma, C. Len, *J. Mol. Catal.* **2020**, *495*, 111133.
[15] F. Wang, C. Yan, R. Jiang, Y. Chen, Y. Wei, Y. Cao, W. Guan, P. Huo, Y. Zhang, *Appl. Clay Sci.* **2023**, *235*, 106872.
[16] Z. Zhang, K. Deng, *ACS Catal.* **2015**, *5*, 6529–6544.
[17] A. D. K. Deshan, L. Atanda, L. Moghaddam, D. W. Rackemann, J. Beltramini, W. O. Doherty, *Front. Chem.* **2020**, *8*, 659.
[18] S. E. Davis, B. N. Zope, R. J. Davis, *Green Chem.* **2012**, *14*, 143–147.
[19] D. Rinsant, G. Chatel, F. Jérôme, *ChemCatChem* **2014**, *6*, 3355–3359.
[20] T. Ishida, K. Kuroda, N. Kinoshita, W. Minagawa, M. Haruta, *J. Colloid Interface Sci.* **2008**, *323*, 105–111.
[21] Y. Cheneviere, V. Caps, A. Tuel, *Appl. Catal. A* **2010**, *387*, 129–134.
[22] R. Saliger, N. Decker, U. Prüße, *Appl. Catal. B* **2011**, *102*, 584–589.
[23] A. Y. Sidorenko, A. V. Kravtsova, A. Aho, I. Heinmaa, K. P. Volcho, N. F. Salakhutdinov, V. E. Agabekov, D. Yu Murzin, *ChemCatChem* **2018**, *10*, 3950–3954.
[24] S. E. Davis, L. R. Houk, E. C. Tamargo, A. K. Datye, R. J. Davis, *Catal. Today* **2011**, *160*, 55–60.
[25] G. J. Hutchings, *ACS Cent. Sci.* **2018**, *4*, 1095–1101.
[26] A. A. Pimerzin, A. Vutolkina, N. Vinogradov, V. Vinokurov, Y. M. Lvov, A. Glotov, *Catal. Today* **2022**, *397*, 121–128.
[27] Y. Wan, J. M. Lee, *ACS Catal.* **2021**, *11*, 2524–2560.
[28] C. Chen, L. Wang, B. Zhu, Z. Zhou, S. I. El-Hout, J. Yang, J. Zhang, *J. Energy Chem.* **2021**, *54*, 528–554.
[29] V. N. Pham, S. Lee, D. T. Hoang, J. Baik, H. S. Kim, H. Lee, *Inorg. Chem.* **2023**, *62*, 12913–12919.
[30] B. D. Terry, J. L. DiMeglio, J. P. Cousineau, B. M. Bartlett, *ChemElectroChem* **2020**, *7*, 3776–3782.
[31] F. Yang, J. Liu, B. Li, H. Li, Z. Jiang, *Biotechnol. Biofuels Bioprod.* **2023**, *16*, 164.
[32] A. O. Karatavuk, *Org. Biomol. Chem.* **2021**, *19*, 10617–10621.
[33] Y. Feng, Y. He, X. Lin, M. Xie, M. Liu, Y. Lvov, *Adv. Healthcare Mater.* **2023**, *12*, 2202265.
[34] Y. Zhao, W. Kong, Z. Jin, Y. Fu, W. Wang, Y. Zhang, J. Liu, B. Zhang, *Appl. Energy* **2018**, *222*, 180–188.
[35] L. Lisuzzo, G. Cavallaro, S. Milioto, G. Lazzara, *J. Colloid Interface Sci.* **2022**, *608*, 424–434.
[36] T. Liu, J. Zhang, P. Ouyang, L. Fu, H. Yang, *Appl. Clay Sci.* **2021**, *215*, 106303.
[37] G. Cavallaro, S. Milioto, G. Lazzara, *Langmuir* **2020**, *36*, 3677–3689.
[38] V. Vergaro, E. Abdullayev, Y. M. Lvov, A. Zeitoun, R. Cingolani, R. Rinaldi, S. Leporatti, *Biomacromolecules* **2010**, *11*, 820–826.
[39] X. Lei, Y. Zhou, X. Liu, L. Kong, L. Liao, Y. Li, M. Liu, L. Tian, W. Rao, G. Lv, *Appl. Clay Sci.* **2023**, *232*, 106799.
[40] Y. Zhang, L. Bai, C. Cheng, Q. Zhou, Z. Zhang, Y. Wu, H. Zhang, *Appl. Clay Sci.* **2019**, *182*, 105259.
[41] M. Mehdizadeh, S. Sadjadi, A. Poater, A. Mansouri, N. Bahri-Laleh, *J. Mol. Liq.* **2022**, *352*, 118675.
[42] A. Y. Sidorenko, Y. M. Kurban, A. Aho, Z. V. Ihnatovich, T. Kuznetsova, I. Heinmaa, D. Y. Murzin, V. Agabekov, *J. Mol. Catal.* **2021**, *499*, 111306.
[43] F. Ferrante, N. Armata, G. Lazzara, *J. Phys. Chem. C* **2015**, *119*, 16700–16707.
[44] F. Ferrante, N. Armata, G. Cavallaro, G. Lazzara, *J. Phys. Chem. C* **2017**, *121*, 2951–2958.
[45] R. Rozza, N. Armata, G. Lazzara, F. Parisi, F. Ferrante, *J. Phys. Chem. C* **2019**, *123*, 10451–10461.
[46] R. Rozza, F. Ferrante, *Appl. Clay Sci.* **2020**, *190*, 105589.
[47] F. Ferrante, M. Bertini, C. Ferlito, L. Lisuzzo, G. Lazzara, D. Duca, *Appl. Clay Sci.* **2023**, *232*, 106813.
[48] L. Lisuzzo, M. Bertini, G. Lazzara, C. Ferlito, F. Ferrante, D. Duca, *Appl. Clay Sci.* **2023**, *245*, 107121.
[49] A. Stavitskaya, E. Khusnetdenova, V. Vinokurov, Y. Lvov, R. Fakhrullin, *Chem. Commun.* **2022**, *58*, 7719–7729.
[50] G. S. Svenningsen, R. Kumar, C. E. Wyman, P. Christopher, *ACS Catal.* **2018**, *8*, 5591–5600.
[51] J. Zhang, V.-A. Glezakou, R. Rousseau, M.-T. Nguyen, *J. Chem. Theory Comput.* **2020**, *16*, 3947–3958.
[52] B. Hourahine, B. Aradi, V. Blum, F. Bonafé, A. Buccheri, C. Camacho, C. Cevallos, M. Y. Deshaye, T. Dumitrică, A. Dominguez, S. Ehlert, M. Elstner, T. van der Heide, J. Hermann, S. Irle, J. J. Kranz, C. Köhler, T. Kowalczyk, T. Kubař, I. S. Lee, V. Lutsker, R. J. Maurer, S. K. Min, I. Mitchell, C. Negre, T. A. Niehaus, A. M. N. Niklasson, A. J. Page, A. Pecchia, G. Penazzi, M. P. Persson, J. Řezáč, C. G. Sánchez, M. Sternberg, M. Stöhr, F. Stuckenberg, A. Tkatchenko, V. W. Yu, T. Frauenheim, *J. Chem. Phys.* **2020**, *152*, 124101.
[53] Y. Sun, S. Liu, X. Guo, S. Huang, *Comput. Theor. Chem.* **2019**, *11–16*, 1154.
[54] C. Bannwarth, S. Ehlert, S. Grimme, *J. Chem. Theory Comput.* **2019**, *15*, 1652–1671.

[55] L. W. Chung, W. M. C. Sameera, R. Ramozzi, A. J. Page, M. Hatanaka, G. P. Petrova, T. V. Harris, X. Li, Z. Ke, F. Liu, H. B. Li, L. Ding, K. Morokuma, *Chem. Rev.* **2015**, *115*, 5678–5796.

[56] M. J. Frisch, G. W. Trucks, H. B. Schlegel, G. E. Scuseria, M. A. Robb, J. R. Cheeseman, G. Scalmani, V. Barone, G. A. Petersson, H. Nakatsuji, X. Li, M. Caricato, A. V. Marenich, J. Bloino, B. G. Janesko, R. Gomperts, B. Mennucci, H. P. Hratchian, J. V. Ortiz, A. F. Izmaylov, J. L. Sonnenberg, D. Williams-Young, F. Ding, F. Lipparini, F. Egidi, J. Goings, B. Peng, A. Petrone, T. Henderson, D. Ranasinghe, V. G. Zakrzewski, J. Gao, N. Rega, G. Zheng, W. Liang, M. Hada, M. Ehara, K. Toyota, R. Fukuda, J. Hasegawa, M. Ishida, T. Nakajima, Y. Honda, O. Kitao, H. Nakai, T. Vreven, K. Throssell, J. A. Montgomery, Jr., J. E. Peralta, F. Ogliaro, M. J. Bearpark, J. J. Heyd, E. N. Brothers, K. N. Kudin, V. N. Staroverov, T. A. Keith, R. Kobayashi, J. Normand, K. Raghavachari, A. P. Rendell, J. C. Burant, S. S. Iyengar, J. Tomasi, M. Cossi, J. M. Millam, M. Klene, C. Adamo, R. Cammi, J. W. Ochterski, R. L. Martin, K. Morokuma, O. Farkas, J. B. Foresman, D. J. Fox, Gaussian 16 Revision C.01 **2016**, gaussian Inc. Wallingford CT.

[57] Y. Zhao, D. G. Truhlar, *Theor. Chem. Acc.* **2008**, *120*, 215–241.

[58] S. Li, S. Tao, F. Wang, J. Hong, X. Wei, *Mikrochim. Acta* **2010**, *169*, 73–78.

[59] P. J. Lin, C. H. Yeh, J. C. Jiang, *RSC Adv.* **2021**, *11*, 36257–36264.